Comparative study of theoretical methods for nonequilibrium quantum transport

J Eckel[1], F Heidrich-Meisner[2], S G Jakobs[3,4], M Thorwart[1], M Pletyukhov[3,4] and R Egger[5]

[1]Freiburg Institute for Advanced Studies (FRIAS), Albert-Ludwigs-Universität Freiburg, 79104 Freiburg, Germany

[2]Department of Physics, Arnold Sommerfeld Center for Theoretical Physics, and Center for NanoScience, Ludwig-Maximilians-Universität München, D-80333 München, Germany

[3]Institut für Theoretische Physik A, RWTH Aachen, 52056 Aachen, Germany

[4]JARA – Fundamentals of Future Information Technologies, RWTH Aachen, 52056 Aachen, Germany

[5]Institut für Theoretische Physik, Heinrich-Heine-Universität Düsseldorf, 40225 Düsseldorf, Germany

Abstract. We present a detailed comparison of three different methods designed to tackle nonequilibrium quantum transport, namely the functional renormalization group (fRG), the time-dependent density matrix renormalization group (tDMRG), and the iterative summation of real-time path integrals (ISPI). For the nonequilibrium single-impurity Anderson model (including a Zeeman term at the impurity site), we demonstrate that the three methods are in quantitative agreement over a wide range of parameters at the particle-hole symmetric point as well as in the mixed-valence regime. We further compare these techniques with two quantum Monte Carlo approaches and the time-dependent numerical renormalization group method.

1. Introduction

Nowadays possibilities of miniaturization down to the nanometer scale allow for studying the single electron transport in ultra-small devices such as, e.g., artificially designed molecular quantum dots [1, 2, 3, 4, 5] or nanotubes, with nontrivial emergent physics such as Fermi-liquid behaviour in quantum dots [6]. Quantum many-body systems driven to nonequilibrium tend to approach a stationary state being distinct in character from their ground state properties [7, 8]. The details of the stationary state may in principle depend on the way how the system is driven out of equilibrium and on the character of the correlations in the system. There is a broad variety of interesting effects when a large bias voltage beyond the regime of linear response is applied to the system due to interaction effects or due to the nonequilibrium conditions [9, 10, 11]. These features range from coherent transport properties, such as, e.g., resonant tunneling, to the Kondo effect. A prominent nontrivial model to study the

interplay of correlation effects and quantum transport is the single impurity Anderson model [12]. This model is believed to capture essential features of experiments with quantum dots [13, 14]. Applying a finite bias voltage across the impurity region allows one to study nonequilibrium effects. This regime is defined by the breakdown of the standard approach of linear response theory when the transport voltage becomes too large.

There are different approximative approaches to deal with the nonequilibrium situation. For example, quantum transport through a quantum dot in the Kondo regime has been described theoretically by Fermi-liquid theory for the asymptotic low-energy regime [15], by means of interpolative perturbation schemes [16], by exploiting the integrability of the model [17, 18], and in terms of the non-crossing approximation [19, 20]. Moreover, there exists a large class of renormalization group approaches which are based on an expansion in the (renormalized) system-reservoir coupling and therefore allow for a treatment of the weak-tunneling regime. For example, the Anderson dot in the charge fluctuation regime [21] and the time evolution of the spin-boson model [22] have been initially considered in an early application of the real-time RG (RTRG) method in its real-time formulation [23]. Nonequilibrium extensions of the perturbative renormalization group [24, 25, 26] and of the flow equation approach [27] as well as the field-theoretical RG approach focusing on the Callan-Symanzik equation [28] have been applied to the nonequilibrium Kondo effect. A more refined analytical perturbative scheme based on a reformulation of the RTRG in frequency space (RTRG-FS) [29] provides a systematic and self-consistent treatment of observables [30] and correlation functions [31] in the nonequilibrium stationary state. Using RTRG-FS, approximate analytic solutions have been proposed for the nonequilibrium Kondo model for weak spin fluctuations [30, 31, 32] and for the interacting resonant level model for weak or strong charge fluctuations [33]. Additionally, the RTRG approach also allows for a description of transient dynamics towards this state [22, 32]. A complementary treatment of transport properties through the Anderson dot can be based upon an expansion in the Coulomb interaction strength [34, 35]. However, bare perturbation theory appears to be insufficient for larger values of the interaction, and therefore, it should be combined with the concept of the renormalization group. The latter prescribes how to renormalize interaction vertices in the nonequilibrium case. This is achieved by combining the Keldysh formalism with the functional renormalization group (fRG) approach in the quantum field theoretical formulation [36, 37, 38, 39]. Very recently, this scheme has been improved by accounting for the frequency dependence of the two-particle vertex [38] in analogy to corresponding developments of the equilibrium Matsubara fRG [40, 41]. As a result of this improvement, the exponentially small scale of the Kondo temperature has partly been observed, namely in the nonequilibrium Fermi-liquid coefficient, that is in the second derivative of the self-energy with respect to bias voltage. Moreover, fRG has been applied to the study of transport properties of a Kondo quantum dot as well [42].

As an alternative to these approaches, numerical methods have been advanced

very recently to properly describe nonequilibrium quantum transport. One important technique is the real-time quantum Monte Carlo method (QMC) [43, 44], which has been extended to non-equilibrium [45, 46, 47, 48, 49]. Although these results are valuable since they are numerically exact, the related calculations are limited to short to intermediate simulation times and the dynamical sign problem often does not allow one to reach the regime of the stationary current for low temperatures. Recent real-time QMC simulations [49] seem to indicate that the splitting of the Kondo resonance which was theoretically predicted earlier in [20, 34] is an artifact of the perturbative approach, consistent with observations from tDMRG [50]. A novel technique based on quantum Monte Carlo (QMC) simulations with complex chemical potentials has been introduced in [51]. This is achieved by an analytic continuation to complex times by employing Matsubara voltages. Then, standard equilibrium quantum Monte Carlo techniques are used in this QMC variant [51, 52]. Beyond raising conceptually fundamental questions, a nonmonotoneous behaviour of the conductance on the bias voltage has been reported [51], whose origin remains unclear and might be attributed to the (arbitrary) choice of the form of the scattering states on which the formalism relies.

Moreover, the multi-layer multi-configuration time-dependent Hartree formalism has recently been introduced [53, 54], which is based on a clever decomposition of the overall Fock space and which has been applied to vibrationally coupled electron transport. In addition, the numerical renormalization group (NRG) method has been very successful in solving quantum impurity problems in equilibrium for several years, see [55] for a topical review. This approach has been generalized to nonequilibrium by using a discrete single-particle scattering basis [56, 57, 58, 59, 60, 61], resulting in the development of the time-dependent numerical renormalization group (TD-NRG). In addition, in [62] and for certain limits of the single impurity Anderson model, a dynamical steady state characterized by correlation induced current oscillations is presented by means of the time dependent density functional theory (TD-DFT).

Furthermore, the adaptive time-dependent density matrix renormalization group method (tDMRG) that generally allows for the simulation of the real-time evolution of pure states in strongly correlated one-dimensional systems [63, 64] has been applied to transport in nanostructures as well [64, 65, 66, 67] and most notably in the present context, to the calculation of current-voltage characteristics of quantum dots [50, 68, 69, 70]. The steady-state currents are computed by taking suitable time-averages over time windows, in which initial transient effects have disappeared already.

Finally, yet another numerical approach has been proposed that is based on the deterministic iterative summation of real-time path integrals (ISPI) [71]. It determines a Keldysh generating function for the time-dependent nonequilibrium current and yields numerically exact results since the systematic errors within the scheme are eliminated exactly. In a first step [71], ISPI was developed for the single-impurity Anderson model and its validity has been confirmed by a detailed comparison with various approximative approaches within their range of applicability.

It is the aim of this work to compare three of these methods, namely, tDMRG, fRG

and ISPI in detail, focusing on steady-state currents as a function of gate potential, voltage bias, temperature, and magnetic field. The goal is to establish their reliability by revealing an excellent quantitative agreement between results obtained with these techniques. We shall further check our results against those of other methods, namely the TD-NRG [59] and two QMC schemes, first the one from [51, 52] and second, the real-time QMC from [47, 49]. In section 2, we introduce the single-impurity Anderson model, which is one the most fundamental models for the description of quantum dots and which we will thus use to benchmark our methods. In section 3, we briefly review the fRG, tDMRG and ISPI schemes. The comparison of the respective numerical results and a discussion are contained in section 4.

2. Model

In what follows we consider the single-impurity Anderson model [12] given by the Hamiltonian ($\hbar = 1$)

$$\begin{aligned}\mathcal{H} &= H_{dot} + H_{leads} + H_T \\ &= \sum_\sigma E_{0\sigma}\hat{n}_\sigma + U\hat{n}_\uparrow\hat{n}_\downarrow + \sum_{kp\sigma}(\epsilon_{kp} - \mu_p)c^\dagger_{kp\sigma}c_{kp\sigma} \\ &\quad - \sum_{kp\sigma}\left[t_p c^\dagger_{kp\sigma}d_\sigma + h.c.\right]. \end{aligned} \tag{1}$$

Here, $E_{0\sigma} = E_0 + \sigma B$ with $\sigma = \uparrow, \downarrow = \pm$ is the energy of a single electron with spin σ on the dot. It can be varied by tuning a back gate voltage or by means of a Zeeman term $\propto B$, under the assumption that the electron dispersion in the leads is not influenced by the magnetic field. The creation/annihilation operator for the dot electron is $d^\dagger_\sigma/d_\sigma$, $\hat{n}_\sigma \equiv d^\dagger_\sigma d_\sigma$ has eigenvalues $n_\sigma = 0, 1$, and the on-dot interaction is U. The energies of the noninteracting electrons in the lead $p = L/R = \pm$ with chemical potential $\mu_p = peV/2$ are denoted by ϵ_{kp} (with fermionic operators $c_{kp\sigma}$). The dot is connected to the leads via the tunnel coupling t_p.

Within the fRG and the ISPI method, we assume the leads to be in thermal equilibrium at temperature T ($k_B = 1$) and moreover take the standard wide-band limit with a constant density of states, $\rho(\epsilon_F)$, around the Fermi energy, yielding the hybridization $\Gamma_p = \pi\rho(\epsilon_F)|t_p|^2$. In this work, we assume symmetric contacts, i.e., $\Gamma_L = \Gamma_R \equiv \Gamma/2$ and we scale all quantities with respect to Γ. The observable of interest is the symmetrized tunneling current $I = (I_L - I_R)/2$ with

$$I(t) = -\frac{ie}{2}\sum_{kp\sigma}\left[pt_p\langle c^\dagger_{kp\sigma}d_\sigma\rangle_t - pt^*_p\langle d^\dagger_\sigma c_{kp\sigma}\rangle_t\right], \tag{2}$$

where $I_p(t) = -e\dot{N}_p(t)$ with $N_p(t) = \langle\sum_{k\sigma} c^\dagger_{kp\sigma}c_{kp\sigma}\rangle_t$. The asymptotic long-time limit gives the stationary steady-state dc current as $I = \lim_{t\to\infty} I(t)$.

3. Methods

Next, we briefly review the three techniques that we want to compare.

3.1. fRG

A detailed explanation on how we apply the fRG to the single-impurity Anderson model is given in reference [37]. Here we only sketch the main ideas.

Spectral as well as transport properties of the model can be comprehensively described if an interaction contribution to the single-particle self-energy Σ is somehow established [19]. A basic idea of the fRG approach consists of a formulation of a flow equation for Σ accounting for its full frequency dependence (therefore this RG approach is called *functional*). The starting point of the flow is the noninteracting limit where the solution is known exactly. During the fRG flow the form of Σ is continuously transformed, and the solution of an interacting problem is achieved when the flow terminates.

Technically, this procedure is set up by artificially making the bare propagator g depend on a flow parameter λ. Being functionals of the bare propagator, the interacting Green's and vertex functions acquire a dependence on λ as well, which is described by an infinite hierarchy of coupled flow equations [72]. In this paper we focus on the flow of the one-particle irreducible vertex functions [73, 74] which has proven to provide a successful approach to the physics of several low-dimensional correlated electron problems [75, 76]. The one-particle irreducible n-particle vertex function can be defined diagrammatically as the sum of all one-particle irreducible diagrams with n amputated incoming lines and n amputated outgoing lines. Here we refer to diagrammatic perturbation theory on the Keldysh contour which results from an expansion in powers of the two-particle interaction U.

We truncate the hierarchy of flow equations by neglecting the flow of the three-particle vertex function. The flow equations for the self-energy Σ^λ and the two-particle vertex function γ^λ then read

$$\frac{d}{d\lambda}\Sigma^\lambda_{1'|1} = -\frac{i}{2\pi}\gamma^\lambda_{1'2'|12}\, S^\lambda_{2|2'} \tag{3}$$

$$\begin{aligned}\frac{d}{d\lambda}\gamma^\lambda_{1'2'|12} = {}& \frac{i}{2\pi}\gamma^\lambda_{1'2'|34}\, S^\lambda_{3|3'}\, G^\lambda_{4|4'}\, \gamma^\lambda_{3'4'|12} + \frac{i}{2\pi}\gamma^\lambda_{1'4'|32}\left[S^\lambda_{3|3'}\, G^\lambda_{4|4'} + G^\lambda_{3|3'}\, S^\lambda_{4|4'}\right]\gamma^\lambda_{3'2'|14} \\ & - \frac{i}{2\pi}\gamma^\lambda_{1'3'|14}\left[S^\lambda_{3|3'}\, G^\lambda_{4|4'} + G^\lambda_{3|3'}\, S^\lambda_{4|4'}\right]\gamma^\lambda_{4'2'|32},\end{aligned} \tag{4}$$

where indices occurring twice in a product imply summation over state and Keldysh indices and integration over independent frequencies. Furthermore, G^λ is the full single-particle propagator and $S^\lambda = -G^\lambda\left[d(g^\lambda)^{-1}/d\lambda\right]G^\lambda$ denotes the so-called single scale propagator.

As flow parameter we use the hybridization constants Γ_p by setting

$$\Gamma_p^\lambda = \Gamma_p + \lambda\frac{\Gamma_p}{\Gamma}, \quad p = L, R, \tag{5}$$

where λ flows from infinity to zero. This choice for the flow parameter ensures the validity of causal properties and of the fluctuation dissipation theorem in the special case of thermal equilibrium [77]. The latter is important in order to reproduce the Fermi liquid behaviour of the model near the particle-hole symmetric point. We approximate the coupling of the three channels in the flow equation (4) of the two-particle vertex by reducing the influence of each channel onto the other two to a renormalization of the interaction strength U. This leads to a frequency dependence of the two-particle vertex of the form

$$\gamma^\lambda(\Pi, X, \Delta) \simeq \overline{v} + \varphi_1^\lambda(\Pi) + \varphi_2^\lambda(X) + \varphi_3^\lambda(\Delta), \tag{6}$$

where $\Pi = \omega_1 + \omega_2 = \omega_1' + \omega_2', X = \omega_2' - \omega_1 = \omega_2 - \omega_1', \Delta = \omega_1' - \omega_1 = \omega_2 - \omega_2'$ are bosonic frequencies corresponding to energy exchange in different channels. In particular, Π refers to the particle-particle and X to the exchange particle-hole channel, while Δ indicates the direct particle-hole channel. A similar approximation has been investigated in studies of the single impurity Anderson model based on the equilibrium Matsubara fRG [41]. In (6), $\overline{v}$ is the bare interaction vertex which is the initial value at the beginning of the flow, and $\varphi_{1,2,3}^\lambda$ are approximations to the corresponding parts of γ produced by the flow equation, see [37]. This approximation considerably reduces the number of sampling points in frequency space which are required for the numerical solution of the flow equation.

3.2. tDMRG

The adaptive time-dependent DMRG method [63, 64] allows for the simulation of the time-evolution of pure states $|\psi(t)\rangle$ at zero temperature (note that generalizations to mixed states and finite temperatures are possible, for a review, see [78] and references therein). The basics of the technique itself are described in the original publications [63, 64] and the review [79]. In a nutshell, the key ingredient of the method is to represent the wave-function in a truncated, but optimized basis instead of the exponentially large basis of the full Hilbert space (see [78] for details). The application of tDMRG to transport in nanostructures was pioneered in [50, 66, 67, 68, 69, 70]. We use the set-up of [50, 67], which we shall briefly summarize.

In contrast to ISPI and fRG, we here apply tDMRG to a real-space representation of the Hamiltonian, i.e., we replace the terms in (1) describing the leads and the hybridization by

$$\begin{aligned} H_{\text{leads}} + H_T = & -t_p \sum_{l=R,L;\sigma} (d_\sigma^\dagger c_{l,1,\sigma} + h.c.) \\ & - \frac{W}{4} \sum_{n=1;l=R,L;\sigma}^{N_{L,R}} (c_{l,n\sigma}^\dagger c_{l,n+1\sigma} \; + \; h.c.)\,. \end{aligned} \tag{7}$$

Moreover, we work on finite systems with open boundary conditions. $N_{L(R)}$ is the number of sites in the left (right) lead, with $N = N_L + N_R + 1$. The hopping matrix element in the leads is $W/4$, where W is the bandwidth. In the present case of a

semielliptical density of states, we obtain $\Gamma = 2t_p^2/(W/4)$ for the hybridization. Note that the leads can also be modeled with other density of states by a different choice of (typically site-dependent) hopping matrix elements in the leads. A prominent example is the logarithmic discretization which is the standard choice in NRG, recently used in some tDMRG simulations as well [69, 80].

A simulation then starts by computing the ground state of (7), defining the initial state $|\psi_0\rangle$, and then, at time $t = 0$, the system is driven out of equilibrium by applying on-site energies $\pm eV/2$ in the leads, mimicking the bias

$$H_{\text{bias}} = \frac{eV}{2} \sum_{n=1}^{N_R} n_{R,n} - \frac{eV}{2} \sum_{n=1}^{N_L} n_{L,n} \,. \tag{8}$$

For the time-evolution $|\psi(t)\rangle = \exp(-iHt/\hbar)|\psi_0\rangle$, we use a Trotter-Suzuki breakup of the time-evolution operator with a time-step of $\delta t = 0.1$ in units of $1/(W/4)$. During the time-evolution, we measure the symmetrized tunneling current $I(t)$, (2). Some typical results for the real-time data are shown in figure 1. As a function of time, $I(t)$ goes through a transient regime before a steady-state is reached. The transient time, besides its dependence on Γ (and, in the Kondo regime on the Kondo temperature T_K), is proportional to $1/V$ [50]. The steady-state regime can be accessed in tDMRG simulations if the typical transient times are smaller than N/v_F, where v_F is the Fermi velocity in the leads. At present, time scales of about $10/\Gamma$ can easily be reached at intermediate bias voltages as figure 1 illustrates (see also the discussion in [50]). The final result of a simulation is, for our purpose, the steady-state current that is computed by taking time-averages over the real-time data. Methods to identify the quasi-steady-state and for finding the correct time-windows for averaging are discussed in [50, 66] and we refer the reader to [50, 66, 81] for a discussion of the time scales governing the transient regime.

The numerical errors inherent to the technique depend on two control parameters, first, the time-step δt and second, the discarded weight $\delta\rho$ [78]. The latter is a measure of the truncation that the wave-function has been subjected to. In the example studied here, the discarded weight is the relevant quantity [50]. Moreover, finite-size effects need to be taken into account and thus runs are carried out for $N \leq 96$ at small biases $V/t \lesssim 0.4$ and $N \leq 64$ at large biases. All results presented in this work have been extrapolated in $1/N$.

Unlike ground-state DMRG [78], there is no criterion that favourably limits the entanglement encoded in the time-evolved wave-function (see also the discussion in [50] and references therein), rendering the simulation increasingly costly at long times and in particular, for large biases $V \gtrsim W/2$. Qualitatively, the larger the entanglement, the larger the dimension of the truncated basis set needs to be that is used to approximate $|\psi(t)\rangle$. This is at present the most crucial limitation of the method. Nevertheless, tDMRG has been very successful in yielding current-voltage characteristics for two of the most basic models used to describe quantum dots, the interacting resonant level model [68] and the single-impurity Anderson model [50].

3.3. ISPI

The ISPI scheme [71] is an in principle numerically exact method to deal with nonequilibrium transport through correlated quantum systems. The method is based on the evaluation of a Keldysh generating function [82], which includes appropriate source terms to generate the observables of interest. Here, this is the nonequilibrium transport current. A real-time path integral

$$Z[\eta] = \int \mathcal{D}\left[\prod_{\sigma} \bar{d}_\sigma, d_\sigma, \bar{c}_{kp\sigma}, c_{kp\sigma}\right] e^{iS[\bar{d}_\sigma, d_\sigma, \bar{c}_{kp\sigma}, c_{kp\sigma}]}, \tag{9}$$

with Grassmann fields $(\bar{d}, d, \bar{c}, c)$ (here we use the same symbols for the Grassmann fields and the fermionic operators in (1)) is constructed for the generating function. The action S corresponds to the Hamiltonian (1) and an external source term is added to the action that allows for computing the dc current at measurement time t_m via $I(t_m) = -i\frac{\partial}{\partial \eta} \ln Z[\eta]\Big|_{\eta=0}$. The full real-time evolution is computed by successively inserting t_m at different Trotter slices, e.g. in [71], figure 5 therein. Next, the path integral is Trotter discretized along the Keldysh contour. The interaction (U-) term is decoupled via a discrete Hubbard-Stratonovich transformation on each single Trotter slice, by which an auxiliary "spin"-field is introduced. For the single-impurity Anderson model, it can assume the values ± 1. Then, all fermionic fields can be integrated out analytically. The remaining task is to perform the summation over all configurations of the (bosonic) auxiliary fields, reminiscent of a discrete path summation. Hence, in

$$Z[\eta] = \sum_{\{s\}} \prod_{\sigma} (-i \det G_\sigma^{-1}[\{s\}, \eta]), \tag{10}$$

(with the total effective Keldysh Green's function G_σ^{-1}), the summation over all configurations s is performed numerically in a deterministic way. The key ingredient for this is the fact that the fermionic environment (the leads) induces non-local correlations in time which decay exponentially in the long-time limit for any finite temperature. This implies the existence of a characteristic memory time up to which all correlations are fully taken into account and beyond which they can be safely neglected for larger times, similar to the case of the spin-boson model [83]. This allows us to disentangle the complete path sum and to construct an iterative scheme to evaluate the generating function. By means of a properly chosen extrapolation procedure, both systematic numerical errors of the scheme, namely the Trotter error and the error due to the finite memory-time, are eliminated. If the extrapolation scheme will be convergent, one is left with the desired numerically exact values for the observable at a fixed measurement time. Convergence is generally problematic when both T and V approach zero. For more details, we refer the reader to [71].

4. Results and Discussion

For the comparison of the three approaches, we compute the symmetrized steady-state current (2). A comparison of the fRG and the tDMRG results has already been shown in [50] for zero temperature and both at particle-hole symmetry and in the mixed valence regime. Consistency between these two methods could be demonstrated for $U/\Gamma \leq 8$ and $eV > T_K$, where T_K is the Kondo temperature. We now set out to include ISPI results into this comparison, starting with the zero temperature transport at the symmetric point $E_0 = -U/2$ at finite on-dot interaction U. We shall then extend our study to the mixed valence regime $E_0 \neq -U/2$, and end up with including a finite magnetic field and finite temperatures, presenting new data from all three methods.

In figure 2, we show the results for the particle-hole symmetric point, $E_0 = -U/2$, of the single-impurity Anderson model. For the case of $U/\Gamma = 2$ we find an excellent agreement between the three methods and with the results from the nonequilibrium real-time QMC approach of [47]. The fRG is expected to be very reliable for $U/\Gamma = 2$ and we can thus use fRG to benchmark the other methods in this limit. Generally (the same applies to the following figures as well), the deviations at large bias voltages between tDMRG on the one hand and fRG and ISPI on the other hand are due to the finite bandwidth used in the tDMRG calculations, as compared to the wide-band limit taken in the other two techniques (see [50] for details). For the large bias voltage (around $eV/\Gamma \sim 4$) tDMRG and ISPI deviate from each other by up to 4%. The high accuracy of the ISPI data is illustrated by our findings shown in figure 2, where the method agrees very well with both the fRG and the tDMRG, to be specific deviations are below 1.5%. For $U/\Gamma = 4$ we find good agreement of the fRG and the tDMRG with the real-time QMC approach from [49]. In the case of $U/\Gamma = 8$, fRG and tDMRG yield very similar results whereas the real-time QMC gives a slightly larger current. Yet these deviations are within the numerical error inherent to the techniques, see e.g. [50].

Next, we compare the results of fRG, ISPI and tDMRG at intermediate interactions and set $U/\Gamma = 3$ (ISPI and fRG are computed at $T = \Gamma/25.6$). The respective current-voltage characteristics $I(V)$ is shown in figure 3 (top). We find a nice agreement over a large range of V, while again, small deviations between ISPI and fRG occur at very large voltages. In figure 3 (bottom), we compare the differential conductance obtained from our three methods with the result of Han and Heary [51] (see figure 2 in that work). We numerically approximate $dI/dV \approx [I(V + \Delta V)] - I(V)/\Delta V$ by choosing a sufficiently small ΔV.

Strong differences between the QMC result and our three techniques occur and the non-monotonous features of the QMC data are not reproduced in our simulations. Moreover, the results of fRG and ISPI coincide at small to intermediate voltages, while some deviations occur at larger voltage ‡. Within the error bars of the numerical differentiation and also taking into account uncertainties in the bare $I(V)$, tDMRG

‡ More recent versions of the method of [51] have given somewhat better agreement [84]. An extensive discussion of this method has recently been presented in [85].

yields results for dI/dV that are consistent with those from fRG and ISPI.

In a next step, we further increase the Coulomb interaction and choose $U/\Gamma = 5$, for which TD-NRG results are available [59]. Using ISPI in its present formulation, this choice for U/Γ does not yet allow us to obtain converged results. In figure 4, we show the results for I from fRG and tDMRG, together with the TD-NRG data by Anders [59]. We find an excellent agreement between fRG and tDMRG for $eV \geq 1.75\Gamma$. The TD-NRG data are very similar to fRG at small bias voltages, while TD-NRG gives larger values for the steady-state current at large values of V than the other two methods. The origin of this discrepancy is, at present, not understood, yet we have reason to speculate that discretization errors may play a role here. tDMRG simulations for an Anderson impurity coupled to Wilson leads, i.e., applied to the same Hamiltonian that NRG treats, also result in too large currents at $eV > T_K$ [69]. Using improved discretization schemes might provide a remedy for this problem and should be tested in future work (see, e.g., [86, 87, 88]).

Next, we address the mixed valence regime for the case of $U/\Gamma = 2$. In figure 5, we show the steady-state current I for different single electron energies $E_0 \neq -U/2$. The results from fRG and ISPI match perfectly from small bias voltages $eV/\Gamma \sim 0.2$ up to the strong non-equilibrium regime. Note that by construction, it becomes increasingly cumbersome (and finally impossible) to obtain converged ISPI results in the limit of vanishing bias voltages and low temperatures [71], since then the correlations do not decay sufficiently fast enough to be truncated. In the present set-up, tDMRG has a tendency to overestimate the currents in the mixed valence regime, for more details, see [50]. This, we believe is the reason for slight deviations from the other two methods (see $eV \approx 1.5\Gamma$, see figure 5, lower left panel). Overall, the agreement between the three methods is obviously still very good, even away from the symmetric point.

Moreover, we consider the case of a finite magnetic field B at the symmetric point, see figure 6. We find an excellent agreement between fRG and ISPI over the full range of bias voltage (deviations are below 1%) and the tDMRG data agree well with the two other methods for $eV \leq 1.5\Gamma$, where we can mimic the wide band limit by keeping $\Gamma, U, B, eV \ll W$.

Finally, in the case of finite temperatures T (see figure 7), for which at present no tDMRG is available yet, we again find a remarkable agreement between fRG and ISPI from the equilibrium up to the strong non-equilibrium case, with deviations below 1.5%. Only at large temperatures both methods tend to disagree slightly for larger bias voltages and deviate up to 10%. We note that for increasing bias voltages, the fRG approach becomes more and more reliable and even asymptotically exact as $V \to \infty$. ISPI also profits from growing bias voltages as they cut off the time non-local correlations in the leads' Green's functions more and more efficiently.

In the remaining part, we wish to point out advantages and disadvantages of the three techniques this work was mainly concerned with, the fRG, tDMRG, and ISPI. fRG is a computationally rather cheap tool to compute current-voltage characteristics over the entire bias range and at practically all temperatures. The approximations

taken in this method have been estimated to be valid up to $U/\Gamma \approx 6$. In particular, in [38] it has been shown that they yield a quantitatively accurate description of the linear conductance as a function of gate voltage, temperature and magnetic field; good descriptions of equilibrium properties of the model have already been observed in Matsubara implementations of the fRG [41, 89]. Concerning nonequilibrium properties, we obtain very good agreement for the nonlinear current and differential conductance for $U/\Gamma \leq 8$ with tDMRG data close to the most critical point $E_0 - U/2 = T = B = 0$ [50]. For sufficiently low (but still finite) temperatures, ISPI yields results that also compare well with fRG. Within the Keldysh fRG framework, we are able to recover [38] the nonequilibrium Fermi-liquid relation [15] and identify an exponentially small energy scale of the Kondo temperature in the corresponding Fermi-liquid coefficient which is the second derivative of the self-energy with respect to bias voltage (although, true Kondo physics for large U/Γ cannot be described in general [38]). However, the reliability of fRG results at larger values of $U/\Gamma \gtrsim 6$ obtained in the scheme truncated at the level of the three-particle vertex is unknown at present, since the justification to truncate the fRG hierarchy of equations can only be given by perturbative arguments. In the single-impurity Anderson model, it is not a priori clear that the contribution of a three-particle vertex is negligible at large U. This constitutes an interesting subject for future research.

Using tDMRG, one can access the finite voltage range with $eV \gtrsim T_K$, as has been demonstrated for $U/\Gamma \lesssim 8$ in [50] and in this work, while the full current-voltage characteristics can be obtained at small $U/\Gamma \sim 4$. The main limitation of the method is the entanglement growth, rendering long time-scales difficult to access at large voltages, which at present excludes an analysis of the deep Kondo regime. A partial solution to this problem is the use of leads with a logarithmic discretization, and then, the correct result is obtained for the linear conductance and $U/\Gamma \lesssim 7$ [69]. tDMRG results can be rendered quite accurate as well, yet since the method requires an exponentially increasing computational time both for reaching long time scales and to obtain very accurate data, in practice, one has to accept a finite numerical error, which can be estimated by tuning control parameters. The greatest advantage of tDMRG is that existing codes can be directly applied to both complex interacting structures as well as interacting leads [90].

Regarding the ISPI scheme, an important advantage is that whenever it converges with respect to its internal control parameters, numerically exact results are obtained, where no sign problem restricts the accessible simulation times and the steady-state regime can directly be reached. In the present implementation, the ISPI scheme converges for sufficiently high temperature *or* sufficiently large bias voltage. The non-local time correlations induced by integrating out the fermions in the leads within this approach become long-ranged only when T and V both approach zero. Such a slow decay of time correlations necessitates a long memory time, i.e., one has to take into account more and more memory slices within the path sum in (10), where the computational effort scales exponentially in the number of memory slices. This problem becomes more

severe for increasing U, and an exploration of the deep Kondo limit remains challenging at present, since the long-range correlations in time are essential for taking into account characteristic features of the Kondo limit. Further improvements of the scheme are under study to allow more efficient calculations in the large-U limit. However, as we have shown above, the present ISPI implementation is able to provide highly accurate and reliable results for $U/\Gamma \lesssim 3$, and the zero temperature limit can be reached for voltages $V \gtrsim 0.1\Gamma$. Moreover ISPI allows for accessing the full real-time characteristics of observables of interest up to in principle asymptotically long times in contrast to real-time QMC approaches [45] where the error bars increase due to the sign problem for long times. It should also be stressed that ISPI is particularly well suited to treat the limit of intermediate-to-high voltages, where alternative methods often run into difficulties.

To summarize, we presented a detailed comparison of theoretical methods designed to model nonequilibrium transport, taking the example of the single-impurity Anderson model. A very encouraging quantitative agreement between the fRG, ISPI, and tDMRG could be established, suggesting that a well-equipped toolbox is available to study nonequilibrium transport in nanostructures. We can also conclude that our methods fair well against alternative developments, namely TD-NRG [59] and two QMC variants [47, 49, 51], of course keeping in mind that not all schemes can be applied in all parameter regimes. In conclusion, each separate approach to nonequilibrium quantum transport bears its own right since different aspects of the real-time dynamics of correlated nonequilibrium quantum systems can be learned from these different approaches.

Acknowledgments

SGJ and MP thank H. Schoeller for numerous valuable discussions on the application of the nonequilibrium fRG, and C. Karrasch and V. Meden for sharing their experience in treating the single impurity Anderson model with fRG methods. JE, MT and RE thank S. Raub for useful technical help with the optimization of the numerical code of the ISPI scheme, and S. Weiss, D. Becker and R. Hützen for useful discussions. FHM acknowledges fruitful discussions with A. Feiguin and E. Dagotto and is indebted to E. Dagotto for granting us computing time at his group's facilities at the University of Tennessee at Knoxville, where the tDMRG simulations were carried out. We further thank F. Anders and the authors of [47] and [49] for sending us their results and V. Meden for comments on a previous version of the text. This work was supported by the DFG Priority Program 1243, by the Excellence Initiative of the German Federal and State Governments and by the DFG Forschergruppe 723. Computational time from the ZIM at the Heinrich-Heine-Universität Düsseldorf is also acknowledged.

References

[1] Reichert J, Ochs R, Beckmann D, Weber H B, Mayor M and v. Löhneysen H 2002 *Phys. Rev. Lett.* **88** 176804

[2] Smit R, Noat Y, Untiedt C, Lang N D, van Hemert M C and Ruitenbeek J M 2002 *Nature* **419** 906
[3] Böhler T, Grebing J, Mayer-Gindner A, v. Löhneysen H and Scheer E 2004 *Nanotechnology* **15** 465
[4] Park H, Park J, Kim A K L, Anderson E H, Alivisatos A P and McEuen P L 2000 *Nature* **407** 57
[5] Park J, Pasupathy A N, Goldsmith J I, Chang C, Yaish Y, Petta J R, Rinkoski M, Sethna J P, Abruna H D, McEuen P L and Ralph D C 2002 *Nature* **417** 722
[6] Potok R M, Rau I G, Shtrikman H, Oreg Y and Goldhaber-Gordon D 2007 *Nature* **446** 167
[7] Abanin D A and Levitov L S 2005 *Phys. Rev. Lett.* **94** 186803
[8] Mitra A and Millis A J 2007 *Phys. Rev.* B **76** 085342
[9] König J, Schmid J, Schoeller H and Schön G 1996 *Phys. Rev.* B **54** 16820
[10] Meir Y and Wingreen N S 1992 *Phys. Rev. Lett.* **68** 2512
[11] Hershfield S, Davies J H and Wilkins J W 1992 *Phys. Rev.* B **46** 7046
[12] Anderson P W 1961 *Phys. Rev.* **124** 41
[13] Goldhaber-Gordon D, Shtrikman H, Mahalu D, Abusch-Magder D, Meirav U, and Kastner M A 1998 Nature (London) **391** 156
[14] van der Wiel W G, Franceschi S D, Fujisawa T, Elzerman J M, Tarucha S, and Kouwenhoven L P 2000 Science **289** 2105
[15] Oguri A 2001 *Phys. Rev.* B **64** 153305
[16] Aligia A A 2006 *Phys. Rev.* B **74** 155125
[17] Konik R M, Saleur H and Ludwig A 2001 *Phys. Rev. Lett.* **87** 236801; Konik R M, Saleur H and Ludwig A 2002 *Phys. Rev.* B **66** 125304
[18] Mehta P and Andrei N 2006 *Phys. Rev. Lett.* **96** 216802; Metha P, po Chao S and Andrei N 2007 preprint arXiv:cond-mat/0703426
[19] Meir Y and Wingreen N S 1993 *Phys. Rev. Lett.* **70** 2601
[20] Wingreen N S and Meir Y 1994 *Phys. Rev.* B **49** 11040
[21] Schoeller H and König J 2000 *Phys. Rev. Lett.* **84** 3686
[22] Keil M and Schoeller H 2001 *Phys. Rev.* B **63** 180302 (R)
[23] Schoeller H 2000, in: Low-Dimensional Systems, p. 137, Lect. Notes Phys., Springer
[24] Kaminski A, Nazarov Y V and Glazman L I 2000 *Phys. Rev.* B **62** 8154
[25] Rosch A, Kroha H, and Woelfle P 2001 *Phys. Rev. Lett.* **87** 156802
[26] Rosch A, Paaske J, Kroha J and Wölfle P 2003 *Phys. Rev. Lett.* **90** 076804
[27] Kehrein S 2005 *Phys. Rev. Lett.* **95** 056602
[28] Doyon B and Andrei N 2006 *Phys. Rev.* B **73** 245326
[29] Schoeller H 2009 Eur. Phys. J. Special Topics **168** 179
[30] Schoeller H and Reininghaus F 2009 *Phys. Rev.* B **80** 045117; *ibid* 2009 *Phys. Rev.* B **80** 209901(E)
[31] Schuricht D and Schoeller H 2009 *Phys. Rev.* B **80** 075120
[32] Pletyukhov M, Schuricht D and Schoeller H 2010 *Phys. Rev. Lett.* **104** 106801
[33] Karrasch C, Andergassen S, Pletyukhov M, Schuricht D, Borda L, Meden V, and Schoeller H 2009 preprint arXiv:0911.5496
[34] Fujii T and Ueda K 2003 *Phys. Rev.* B **68** 155310; 2005 *J. Phys. Soc. Jpn.* **74** 127
[35] Thygesen K S and Rubio A 2008 *Phys. Rev.* B **77** 115333
[36] Gezzi R, Pruschke T, and Meden V 2007 *Phys. Rev.* B**75** 045324
[37] Jakobs S G, Meden V, and Schoeller H 2007 *Phys. Rev. Lett.* **99** 150603
[38] Jakobs S, Pletyukhov M, and Schoeller H 2009 preprint arXiv:0911.5502
[39] Karrasch C, Pletyukhov M, Borda L and Meden V 2009 preprint arXiv:0911.5165, accepted for publication in *Phys. Rev.* B
[40] Hedden R, Meden V, Pruschke T and Schönhammer K 2004 *J. Phys.: Condens. Matter* **16** 5279
[41] Karrasch C, Hedden R, Peters R, Pruschke T, Schönhammer K and Meden V 2008 *J. Phys.: Condens. Matter* **20** 345205
[42] Schmidt H and Wölfle P 2009 *Ann. Phys.* **19** 60

[43] Mak C H and Egger R 1999 *J. Chem. Phys.* **100** 12; Egger R, Mühlbacher L and Mak C. H. 2000 *Phys. Rev.* E **61** 5961
[44] Mühlbacher L and Egger R 2003 *J. Chem. Phys.* **118** 179
[45] Mühlbacher L and Rabani E 2008 *Phys. Rev. Lett.* **100** 176403
[46] Schmidt T, Werner P, Mühlbacher L and Komnik A 2008 *Phys. Rev.* B **78** 235110
[47] Werner P, Oka T and Millis A J 2009 *Phys. Rev.* B **79** 035320
[48] Schiro M and Fabrizio M 2009 *Phys. Rev.* B **79** 153302
[49] Werner P, Oka T, Eckstein M and Millis A J 2010 *Phys. Rev.* B **81** 035108
[50] Heidrich-Meisner F, Feiguin A E and Dagotto E 2009 *Phys. Rev.* B **79** 235336
[51] Han J E and Heary R J 2007 *Phys. Rev. Lett.* **99** 236808
[52] Han J E 2009 preprint arXiv:0906.5577
[53] Härtle R, Benesch C and Thoss M 2008 *Phys. Rev.* B **77** 205314
[54] Wang H and Thoss M 2009 *J. Chem. Phys.* **131** 024114
[55] Bulla R, Costi T A, and Pruschke T 2008 *Rev. Mod. Phys.* **80** 395
[56] Anders F B and Schiller A 2005 *Phys. Rev. Lett.* **95** 196801
[57] Anders F B and Schiller A 2006 *Phys. Rev.* B **74** 245113
[58] Anders F B, Bulla R, and Vojta M 2007 *Phys. Rev. Lett.* **98** 210402
[59] Anders F B 2008 *Phys. Rev. Lett.* **101** 066804; 2008 *J. Phys.: Cond. Matter* **20** 195216
[60] Roosen D, Wegewijs M R, Hofstetter W 2008 *Phys. Rev. Lett.* **100** 087201
[61] Schmitt S and Anders F B preprint arXiv:0909.5555
[62] Kurth S, Stefanucci G, Khosravi E, Verdozzi C and Gross E K U preprint arXiv:0911.3870
[63] Daley A J, Kollath C, Schollwöck U, and Vidal G 2004 *J. Stat. Mech.: Theor. Exp.* P04005
[64] White S R and Feiguin A E 2004 *Phys. Rev. Lett.* **93** 076401
[65] Schmitteckert P 2004 *Phys. Rev.* B **70** 121302
[66] Schneider G and Schmitteckert P, preprint arXiv:cond-mat/0601389
[67] Al-Hassanieh K A, Feiguin A E, Riera J A, Büsser C A and Dagotto E 2006 *Phys. Rev.* B **73** 195304
[68] Boulat E, Saleur H, and Schmitteckert P 2008 *Phys. Rev. Lett.* **101** 140601
[69] Dias da Silva L G G V, Heidrich-Meisner F, Feiguin A E, Büsser C A, Martins G B, Anda E V and Dagotto E 2008 *Phys. Rev.* B **78** 195317
[70] Kirino S, Fujii T and Ueda K 2008 *J. Phys. Soc. Jpn.* **74** 127
[71] Weiss S, Eckel J, Thorwart M and Egger R 2008 *Phys. Rev.* B **77** 195316; *ibid* 2009 **79** 249901(E)
[72] Salmhofer M 1998 *Renormalization: An Introduction* (Heidelberg: Springer)
[73] Wetterich C 1993 *Phys. Lett.* B **301** 90; Morris T R 1994 *Int. J. Mod. Phys.* A **9** 2411.
[74] Salmhofer M and Honerkamp C 2001 *Prog. Theor. Phys.* **105** 1.
[75] Metzner W 2005 *Prog. Theor. Phys. Suppl.* **160** 58.
[76] Meden V 2007 in *Advances in Solid State Physics*, Vol. 46, ed. by Haug R (New York: Springer); arXiv:cond-mat/0604302.
[77] Jakobs S G, Pletyukhov M and Schoeller H 2010 *J. Phys. A: Math. Theor.* **43** 103001
[78] Schollwoeck U 2005 *Rev. Mod. Phys.* **77** 259
[79] Schollwoeck U and White S R 2006, in: Effective models for low-dimensional strongly correlated systems, p. 155, AIP, Melville, New York.
[80] Guo C, Weichselbaum A, Kehrein S, Xiang T, and von Delft J 2009 *Phys. Rev. B* **79** 115137
[81] Schiller A and Hershfield S 2000 *Phys. Rev.* B **62** R16271
[82] Keldysh L V 1964 *Zh. Eksp. Teor. Fiz.* **47** 1515 [1965 *Sov. Phys. JETP* **20** 1018]
[83] Eckel J, Weiss S and Thorwart M 2006 *Eur. Phys. J.* B **53** 91
[84] Han J 2010 private communication
[85] Dirks A, Werner P, Jarrell M and Pruschke T 2010, arXiv:1002.4081
[86] Zitko R 2009 *Comp. Phys. Comm.* **180** 1271
[87] Zitko R and Pruschke T 2009 *Phys. Rev. B* **79** 085106
[88] Weichselbaum A, Verstraete F, Schollwöck U, Cirac J I, and von Delft J 2009 *Phys. Rev. B* **80**

165117
[89] Karrasch C, Enss T and Meden V 2006 *Phys. Rev.* B **73** 235337
[90] Feiguin A E, Fendley P, Fisher M P, and Nayak C 2008 *Phys. Rev. Lett.* **101** 236801

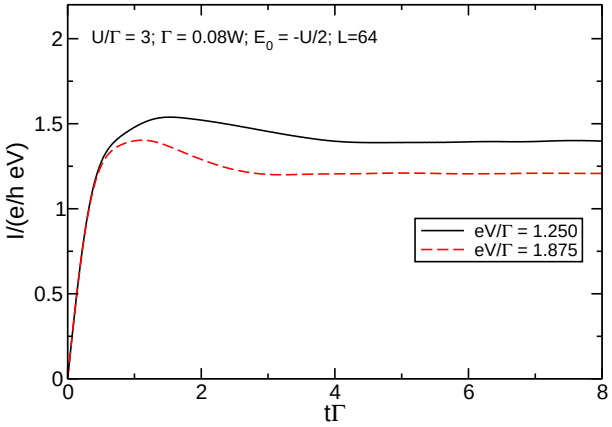

Figure 1. Real-time evolution of the current $I(t)$ at the symmetric point $E_0 = -U/2$ for $U/\Gamma = 3$ for the tDMRG. Real-time results from the ISPI approach can be found in [71], figure 5 therein.

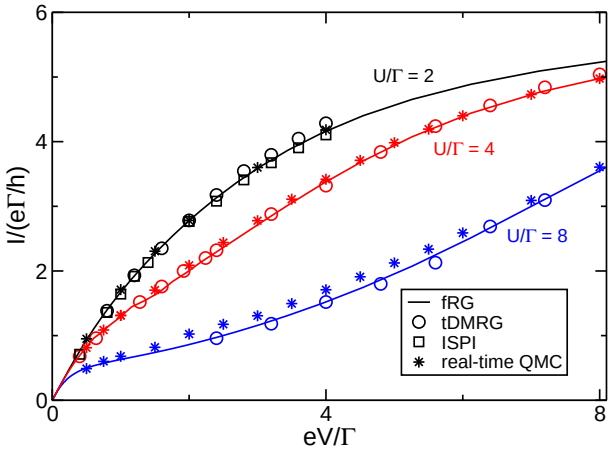

Figure 2. Steady-state current I at the symmetric point $E_0 = -U/2$ for $U/\Gamma = 2$ as a function of the applied bias voltage eV/Γ. The tDMRG results are taken from [50] and were computed for $U = W/8$ (Γ chosen correspondingly) and extrapolated in the inverse system size. The real-time QMC data are taken from [47] ($U/\Gamma = 2$) and [49] ($U/\Gamma = 4$ and 8). In the ISPI approach, we set the temperature to $T = 0.1\Gamma$.

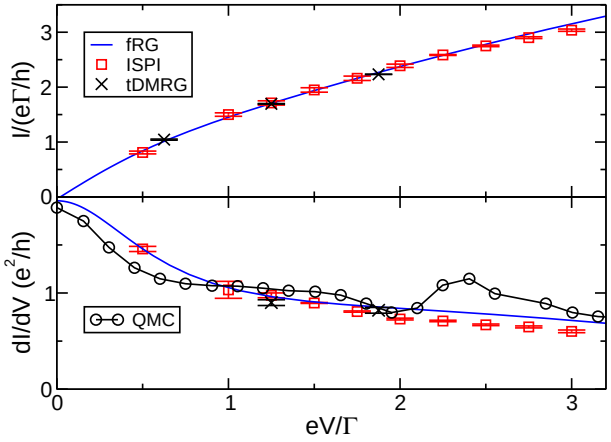

Figure 3. Current-voltage characteristics (top) and differential conductance (bottom) for $U/\Gamma = 3$. The temperature is $T = \Gamma/25.6$ and the remaining parameters are the same as in figure 2. The circles represent the results from a QMC method using an analytic continuation to imaginary Matsubara voltages; [51] (figure 2 therein).

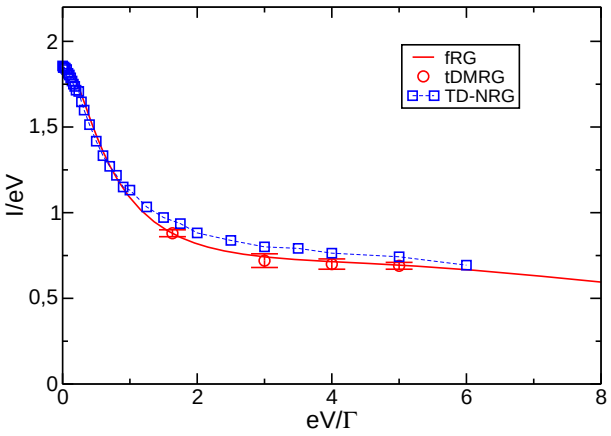

Figure 4. Comparison of the steady-state current I divided by eV for $U/\Gamma = 5$ for the fRG, tDMRG and the TD-NRG [59]. The remaining parameters are the same as in figure 2.

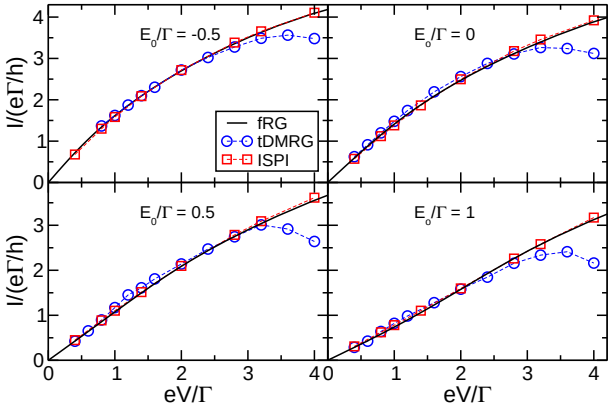

Figure 5. Steady-state current for the mixed valence regime for different single electron energies E_0 with $U/\Gamma = 2$. The remaining parameters are the same as in figure 2. The tDMRG data are taken from [50].

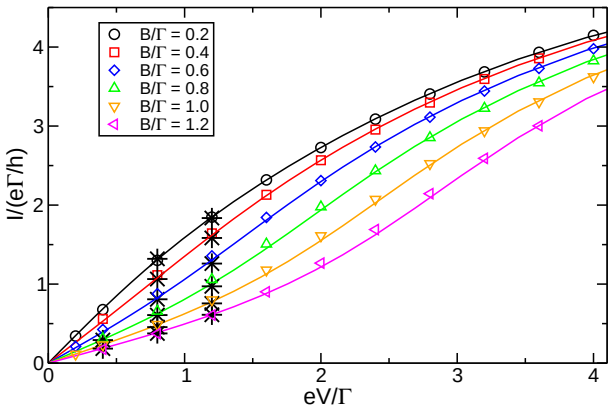

Figure 6. Steady-state current I for finite magnetic field B, remaining parameters are the same as in figure 2. The solid lines are the fRG results corresponding to the symbols of the ISPI results and the corresponding tDMRG results are marked with the black stars.

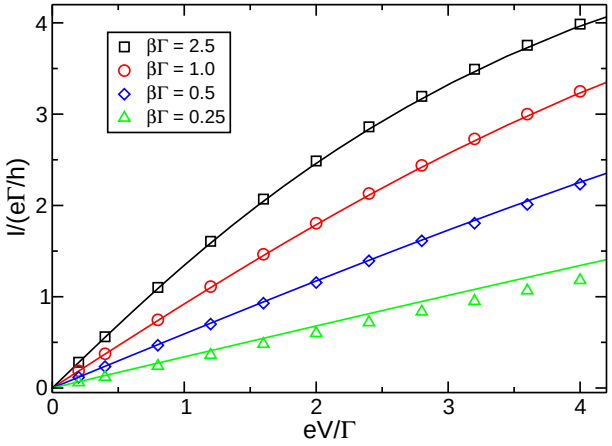

Figure 7. Temperature dependence of the steady-state current. The solid lines correspond to the fRG results, the symbols denote the ISPI results. The remaining parameters are the same as in figure 2, with $\beta = 1/T$ being the inverse temperature.